The potential for additive manufacturing of compact horizontal spiral tube condensers

Nicolaas Steenekamp[1*] and *Gys* Jacobs[1]

[1] Department of Mechanical and Mechatronic Engineering, Central University of Technology, South Africa

Abstract. Research on heat transfer and pressure drop in Archimedean spiral coil heat exchangers is limited, with little focus on condensation applications and flow hydrodynamics. Despite challenges in fabrication, spiral coils offer advantages in compactness and enhanced heat transfer. Although centrifugal forces improve heat transfer, they simultaneously increase pressure losses. Heat transfer correlations for two-phase condensing flow in Archimedean spiral coils remain unpublished. Additive manufacturing offers a promising solution for the fabrication of Archimedean spiral coil heat exchangers. This paper reviews the application of Archimedean spiral coils in compact condensers, the thermo-hydraulic design of spiral coil heat exchangers, and explores the potential of additive manufacturing for their production.

1 Introduction

Inspired by the potential of Organic Rankine Cycle (ORC) technology to harness low-grade waste heat, this paper explores the potential application of Additive Manufacturing (AM) for micro-scale ORC systems (net power output <10 kW). For this study, the focus is on an additively manufactured, Archimedean spiral coil, compact cross-flow, air-cooled condenser.

2 Compact condensers

Compact condensers are used in small industrial processes, research & development, and waste heat recovery processes [1]. A compact surface is defined as having a large heat transfer surface area per unit volume (liquid-to-liquid $\beta \geq 700$ m^2/m^3 and gas-to-liquid $\beta \geq 400$ m^2/m^3) [2]. Compact condensers feature flow passages with hydraulic diameters ranging from 1 mm $\leq D_h \leq 5$ mm. The hydraulic diameter of a tube-fin bundle is defined as the ratio of the cross-sectional area available for flow to the wetted perimeter of the flow path, which is typically observed perpendicular to the axis of the tubes. The hydraulic diameter is directly proportional to the geometric spacing of the tube bundle and the pitch of the fins. Fig. 1 shows the heat transfer surface area density of compact surfaces.

* Corresponding author: steenekampnk@gmail.com

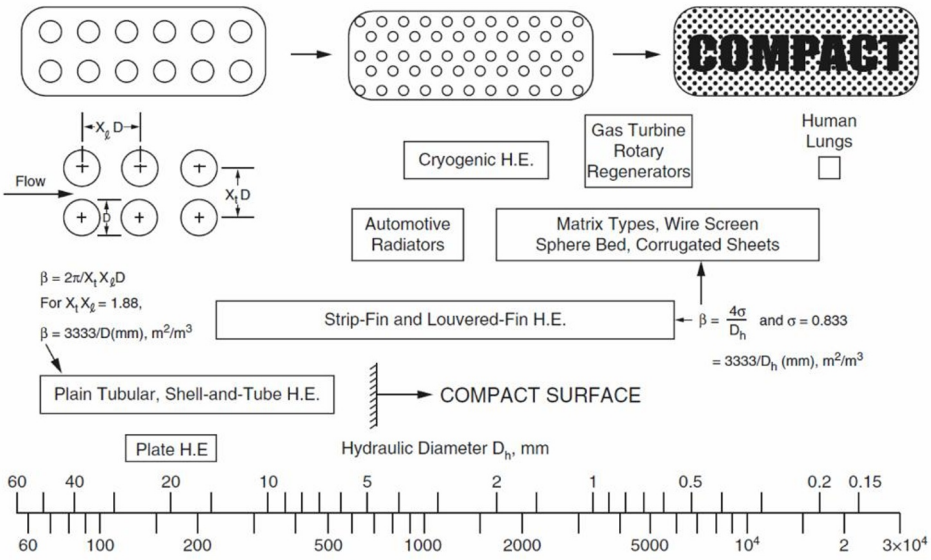

Fig. 1. Heat transfer surface area density β (m^2/m^3) [3].

Fig. 2 shows the relative heat transfer surface area required for each of three flow arrangements namely parallel-, cross-, and counter-flow, as a function of the fluid temperature change.

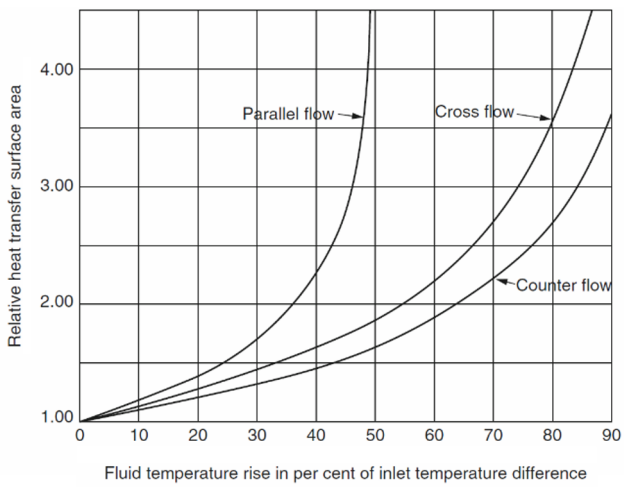

Fig. 2. Relative heat transfer surface area vs. fluid temperature rise [3].

The cross-flow arrangement is the most commonly used for compact heat exchangers in industry, being best suited for extended surface heat exchangers [4], making it ideal for installations with limited space [5]. The counter-flow arrangement is the most efficient in single-pass heat exchangers, while the parallel-flow arrangement is the least efficient [6]. The effectiveness of the cross-flow heat exchanger lies between that of the parallel-flow and counter-flow arrangements.

3 Spiral coil condensers

Condensation in tubes typically requires a long flow path. Hence many small capacity refrigerant condensers employ a long finned serpentine tube, a schematic of a serpentine wire-and-tube condenser is shown in Fig. 3.

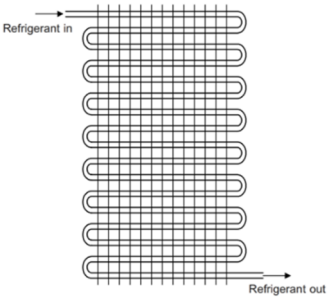

Fig. 3. Schematic of a serpentine wire-and-tube condenser [7].

Tube condensers can be made more compact if a spiral tube configuration is used. Schematics of a helical-coil heat exchanger and Archimedean spiral coil are respectively shown in Fig. 4.

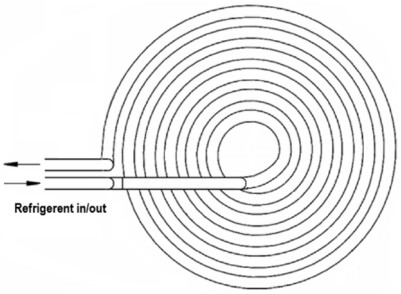

Fig. 4. Schematic of an Archimedean-spiral coil heat exchanger (Adapted from [8]).

Naphon and Wongwises (2003) investigated the thermal performance of spiral coil finned-tube heat exchangers in a cross-flow arrangement. Building on this, Cihan and Kahveci (2015) studied their application as air-cooled condensers [9]. A typical configuration of such a cross-flow helical-coil finned-tube condenser is shown in Fig. 5.

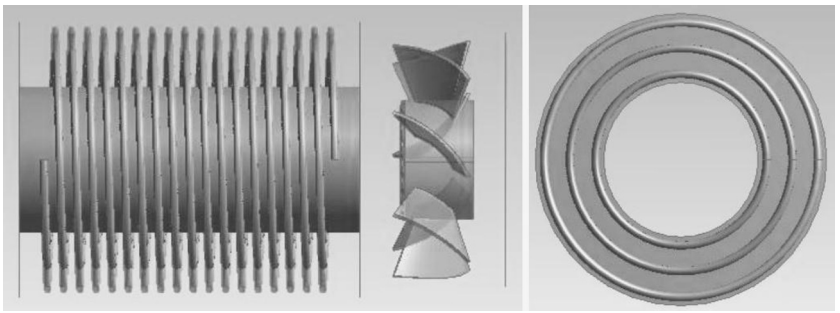

Fig. 5. Configuration of a cross-flow air-cooled helical-coil finned tube condenser studied by Cihan et al. (2015) [9].

Among the various curved coils studied to date, spiral coils have attracted the least research attention, likely due to the challenges associated with their fabrication [10]. AM offers a

solution to rapidly manufacture complex components from computer-aided design (CAD) data that were previously thought to be nearly impossible to produce using conventional methods [11].

4 Additive manufacturing applied to compact spiral condensers

AM refers to a group of technologies that create components by fusing powder particles layer by layer, rather than removing material through conventional subtractive processes [12]. Over the past three decades, AM has transformed the way heat exchangers are designed and manufactured. It enables function-driven optimisation and improves heat transfer performance. AM also enhances compactness and fluid-thermal integration. These benefits help overcome many of the geometric limitations imposed by traditional planar or tubular manufacturing methods [15]. While this flexibility offers many advantages, it also comes with significant limitations regarding the types of features that can be produced. To address such limitations, design guidelines have been developed by researchers, machine manufacturers, and industry consultants. These guidelines aim to prevent common failures and ensure part success on the first print attempt [13], [14], [15]. It is important to recognise that the design of compact heat exchangers is driven not only by thermo-hydraulic performance but also by the capabilities and constraints of the AM process itself [15].

4.1 Geometric flexibility and surface features

Conventional helical coiled tube heat exchangers are often equipped with fins to improve heat transfer. However, these designs are typically limited to using standard off-the-shelf circular tubing (cf. Fig. 6(a)). AM allows for far greater design flexibility. Tube and fin spacing can be adjusted based on specific performance requirements. The cross-sectional shape of the spiral tube also does not need to be circular. It can be customised to improve heat transfer. Additional surface features can also be incorporated along the tube wall. These include dimples (cf. Fig. 6(b)), twisting (cf. Fig. 6(c)), or other geometric modifications. Such enhancements promote turbulence and help increase the heat transfer rate.

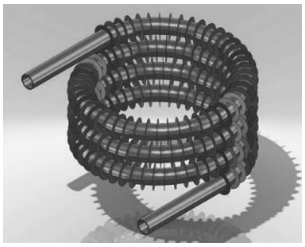

(a) Conventional finned helix-coil heat exchanger tube [16].

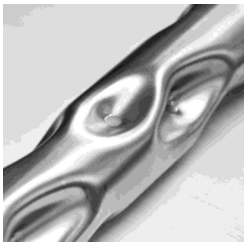

(b) Dimpled straight heat exchanger tube for enhanced heat transfer [17].

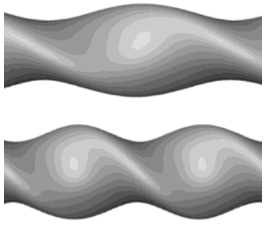

(c) Twisted straight heat exchanger tubes for enhanced heat transfer [16].

Fig. 6. Conventional and enhanced heat exchanger tube geometries.

The finned spiral condenser depicted in Fig. 7 is an example of a configuration that should be readily feasible with additive manufacturing, especially if the intention is to additively manufacture customised condensers for specific working fluids, operating envelopes and heat transfer duties.

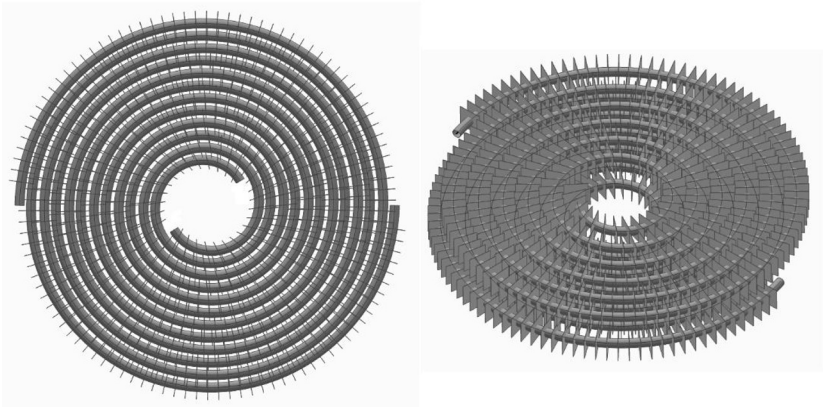

Fig. 7. CAD model views of one of the proposed additively manufactured finned spiral coil condenser configurations.

4.2 Material selection

Table 1 shows a comparison of general properties of AM materials, followed by an overview of the listed materials. A variety of materials are available for heat exchanger manufacturing, with key considerations including density, thermal conductivity, processability, and cost. Material selection depends on component requirements, operational environment, and boundary conditions [15].

Table 1. Comparison of general properties of Additive Manufacturing materials adapted from [15].

No.	Material	Type	Density	Conductivity	Melt	Friendly*
a)	Copper	Cu alloys	8.96 g/cm³	401 W/m·K	1084 °C	4
b)	Aluminium	AlSi10Mg, AlSi12, Aeromet A20X™, Scalmalloy®	2.70 g/cm³	205 W/m·K	660 °C	6
c)	Nickel	Inconel 625 Inconel 718	8.90 g/cm³	94 W/m·K	1453 °C	8
d)	Titanium	Ti6Al4V	4.51 g/cm³	22 W/m·K	1670 °C	9
e)	Stainless	316L	8.00 g/cm³	16 W/m·K	1530 °C	10

Legend: AM Friendly where 1 = poor, 10 = excellent

Copper alloys provide excellent heat transfer capabilities, though they pose challenges in AM. Challenges include low printability due to high surface reflectivity, sensitivity to impurities, potential delamination of layers, and bending arising from high thermal gradients during printing. Recent studies have increased research into AM of copper alloys for heat transfer applications [15].

Aluminium alloys are popular material selection for heat exchangers. Aluminium alloys have high thermal conductivity, low density, and cost-effectiveness compared with other metals [15]. Cast-based aluminium powders are preferred because they reduce defects and exhibit similar properties to conventional castings. The most utilised alloys, AlSi12 and AlSi10Mg are chosen for their weldability, castability, and low shrinkage [18].

Nickel-based alloys are used in aerospace applications. Titanium alloys are recognised for their high strength, low density, fracture toughness, corrosion resistance, and biocompatibility, enabling weight reduction while ensuring reliability. Ongoing research evaluates their processability, including fabricating thin-walled features [15].

Stainless steels are preferred for aeronautical and aerospace applications. The mechanical property of the material is inherently robust, corrosion resistant, and affordable. Numerous studies address the processability of 316L [15].

4.3 Surface roughness and porosity

Surface roughness enhances heat transfer, but it also enhances heat exchanger fouling. Thin walls are desirable to minimise thermal conductivity resistance. However, heat exchanger walls may not be porous, which will cause leakage. The heat exchanger walls must also be sufficiently thick to withstand the operational pressures prevalent in the heat exchanger.

Shange et al. (2019) investigated the relationship between the inclination angle and orientation of laser powder bed fused (LPBF) manufactured parallel-piped samples, and the resulting surface roughness and porosity. These deformations can disrupt the distribution of powder layers, increasing the surface roughness and reducing the fatigue life cycle of the produced object [19]. The overall best downskin surface roughness is achieved at inclination angles between 55° and 60°, see Fig. 8. Support structures effectively stabilise surfaces on objects with angles below 45°, however these supports increase the manufacturing time and material wastage post part processing [20][21].

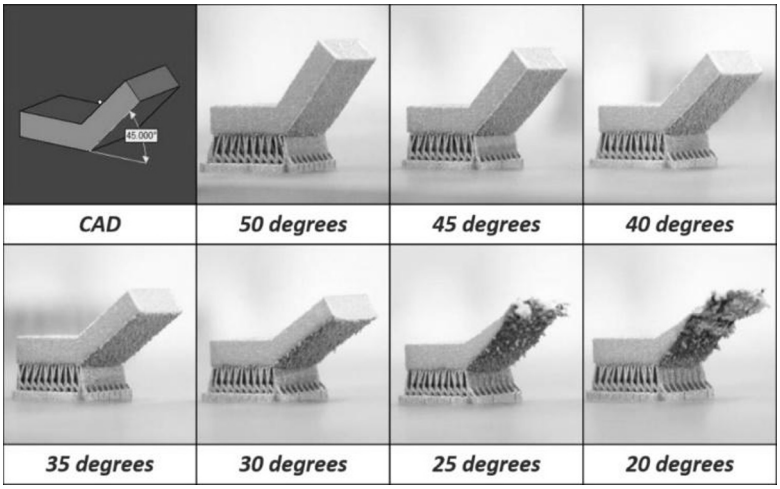

Fig. 8. Manufacturing limits for inclined surfaces adapted from [22].

4.4 Thin features

The design of thin features in AM components requires careful consideration of technological limitations. The current manufacturing limit for direct metal laser sintering (DMLS) for micro-channels and fin thicknesses is approximately 0.15 mm. Despite the growing interest in compact heat exchangers, leakage issues have not been extensively studied [13]. Leak-free features are crucial in heat exchangers, as porosity is a significant concern in fluid systems. Venter et al. (2018) recommended a minimum wall thickness of 0.35 mm, emphasising the importance of this specification in ensuring the structural integrity of components within fluid systems. A thicker wall helps to prevent issues such as porosity and surface flaws, which can compromise the performance of heat exchangers [20].

Moreover, fabricating high-quality, defect-free thin walled features below 0.2 mm to 0.3 mm remains challenging. In contrast, conventional manufacturing methods such as sheet rolling and stamping can produce sheets ranging from 0.046 mm to 0.2 mm in thickness [13]. In contrast, conventional heat exchanger tubes, often referred to as drawn tubes, typically have a wall thickness of 0.56 mm for a 6 mm tube size, corresponding to Birmingham Wire Gauge (BWG) 24 [23]. AM has yet to mature sufficiently for the mass production of thin features critical to heat exchanger performance [13].

4.5 Overhang features

Horizontal channels are prone to deformation without additional support structures [20]. Fig. 9 shows horizontally spaced surfaces featuring unsupported overhang features. Support structures become necessary when the spacing exceeds 2 mm [24]. This limitation makes it challenging to produce horizontally printed circular cross-section flow channels.

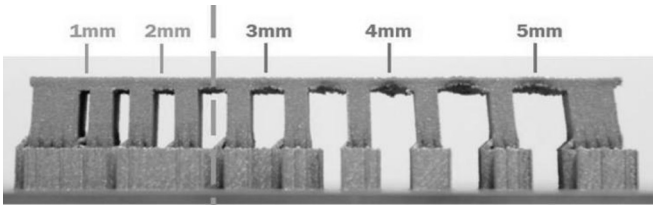

Fig. 9. Overhang limit for non-inclined surfaces adapted from [22].

4.6 Circular features

For circular sections, such as continuous tubes, it is preferable to orient the axis vertically during manufacturing. Although AM software automatically generates supports, optimised supports incorporated within the CAD model can eliminate the need for post-manufacturing material removal. Supports should be added to sections with diameters exceeding 6 mm to ensure an accurate circular profile. In some cases, it is more practical to join parts using bolts and nuts through pre-designed bolt holes rather than performing post-production drilling and tapping. Holes smaller than M10 often exhibit inadequate thread definition and should be produced post-manufacturing by drilling and tapping. However, drilling and tapping threaded holes into materials such as Ti-6Al-4V remains a challenging task [25][20].

4.7 Post-production cleaning

A significant challenge associated with compact heat exchangers is the internal fouling of tubes. Intricate features, such as fins and pins that act as flow inhibitors, cannot be readily cleaned using conventional mechanical methods [26]. Consequently, AM components require thorough cleaning during post-production. The removal of entrapped or unsintered powder from complex internal channels is particularly challenging, especially when the heat exchanger core is fully enclosed. Limited literature addresses this issue; some authors suggest redesigning components or employing specialised equipment and methods. Therefore, heat exchangers should be designed with accessible access ports or ends to facilitate visual inspection and cleaning of the internal structure [20][13].

4.8 Post-production thermal treatment

In DMLS, components often require post-thermal treatments to enhance their material properties. As-fabricated materials typically exhibit inferior microstructures and mechanical properties compared with those produced by conventional methods. The unique thermal cycles associated with AM processes characterised by rapid heating and cooling, induce residual stresses and potential distortion, thereby increasing the risk of damage and malfunction [13].

5 Heat transfer and pressure drop correlations

Spiral coils have been reported to enhance heat transfer compared to traditional straight tubes due to the influence of centrifugal forces [27]; however, this improvement in heat transfer is accompanied by a significant increase in pressure loss [28]. Heat transfer and pressure drop correlations on spiral coils are limited in the scientific literature [10]. The flow pattern and frictional pressure drop of two-phase flow in spiral coils have scarcely been studied [29].

5.1 Single-phase flow correlations

Heat transfer and pressure drop correlations in horizontal straight tubes are not directly applicable to spiral coils, as they do not account for geometric influences of form drag and curvature-induced secondary flows [10]. Nusselt number correlations are required to calculate the expected convective heat transfer coefficients. Without knowledge of the convective heat transfer coefficients a heat exchanger cannot be designed. Publications on the hydrodynamics of flow through spiral coils are limited to single phase flow, and the existing correlations are only valid for smooth tubes [30]. Kubair and Kuloor (1966) developed Nusselt number correlations for laminar flow in spiral coils enclosed in a steam chamber using glycerol solutions. Orlov and Tselishchev (1964) provided Nusselt number correlations for turbulent flow in spiral coils using Mikheev's correlation that uses the average spiral radius of curvature [31].

This suggests most helical coil correlations apply to spiral coils if the average curvature radius is used[1]. . The Chilton–Colburn analogy may be regarded as a purely empirical extension of the Reynolds analogy [32]. It remains one of the most widely accepted and utilised methods in the heat transfer literature. The Chilton and Colburn j-factor has been successfully used in the design of compact heat exchangers; however, this correlation offers limited accuracy when estimating Nusselt numbers from known friction factors in spiral coils [10].

Patil (2019) proposed empirical correlations for heat transfer and pressure drop in spiral coils under laminar and turbulent flow conditions. Patil proposed a revised analogy that incorporate both viscous and form drag effects and demonstrated their validity across a range of Reynolds (Re) and Dean numbers (De) [10]. The average values of friction factors of spiral coil tubes under laminar flow conditions were approximately 24% higher compared to the values of straight tubes. The friction factors of helical coil tubes were approximately 31% higher compared to the values of spiral coil tubes. The Nusselt numbers of helical coil tubes were approximately 20% lower than those of spiral coil tubes under similar conditions [10]. The geometry of a constant pitch spiral coil and tube is shown in Fig. 10. Where P is the constant pitch of the spiral coil, Dci and Dco are the internal and external diameters of the spiral coil, and D_i and D_o are the inner and outer diameters of the tube.

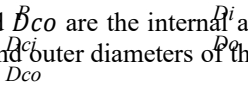

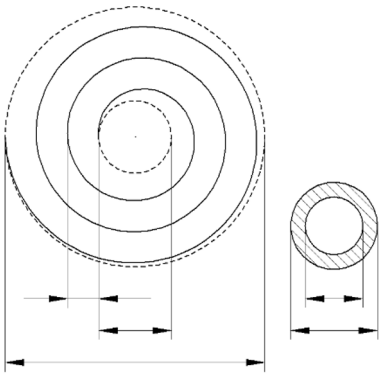

Fig. 10. Geometry of a constant pitch spiral coil and tube.

For laminar flow in spiral coil tubes, the Nusselt number correlation (Nu) is shown in equation (1) and the friction factor correlation (f_c) is shown in equation (2). Both equations depend on the geometrical parameters of the spiral coil.

$$Nu = 1.3374 \cdot De^{0.64} \cdot \left(\frac{D_i}{D}\right)^{0.31} \cdot \left(\frac{P}{D_i}\right)^{-0.11} \cdot Pr^{1/3} \tag{1}$$

In equation (1) D is the average spiral coil diameter, and Pr is the Prandtl number. Equation (1) is valid for 16 < *Re* < 3183; 3 < *De* < 450; 84 < *Pr* < 298; 0.015 < $\frac{\mathrm{D_i}}{\mathrm{D}}$ < 0.029; 1.875 < $\frac{\mathrm{P}}{\mathrm{D_i}}$ < 6.31. Where $D = \frac{\mathrm{Dci+Dco}}{2}$, $De = Re\sqrt{\frac{D_i}{D}}$

$$f_c = 35.157 \cdot De^{-0.91} \cdot \left(\frac{D_i}{D}\right)^{0.78} \cdot \left(\frac{P}{D_i}\right)^{0.11} \tag{2}$$

The friction factor in equation (2) is valid for 8.99 < *Re* < 6696.29; 1.12 < *De* < 878; 0.015 < $\frac{\mathrm{D_i}}{\mathrm{D}}$ < 0.029; 1.875 < $\frac{\mathrm{P}}{\mathrm{D_i}}$ < 6.31

The laminar flow Nusselt numbers and friction factors for spiral coils can be determined with equations (3) and (4), independently, when either is known. The Mean Bias Error (MBE) and Root Mean Square Error (RMSE) was found to be 0.78%, and ± 5.08 % [10].

$$Nu = 0.16\left(\frac{f_c}{2}\right)^{0.40}\left(\frac{D_i}{D}\right)^{0.24}\left(\frac{P}{D_i}\right)^{-0.16} Re \cdot Pr^{1/3} \tag{3}$$

$$\left[\frac{\left(\frac{Nu}{Re \cdot Pr}\right)Pr^{2/3}}{0.16\left(\frac{D_i}{D}\right)^{0.24}\left(\frac{P}{D_i}\right)^{-0.16} Re \cdot Pr^{1/3}}\right]^{\frac{1}{0.40}} = \left(\frac{f_c}{2}\right) \tag{4}$$

For turbulent flow in spiral coil tubes, the Nusselt number and friction factor are obtained with equation (5) and (6), from the Schmidt correlations [33], as cited in Patil [10]:

$$Nu = 0.023\left[1 + 3.6\left(1 - \left(\frac{D_i}{D}\right)\right)\left(\frac{D_i}{D}\right)\right]^{0.8} Re^{0.8} Pr^{1/3} \tag{5}$$

$$f_c = \left[1 + 0.0823\left(1 - \left(\frac{D_i}{D}\right)\right)\left(\frac{D_i}{D}\right)^{0.53} Re^{0.25}\right] \cdot \frac{0.079}{Re^{0.25}} \tag{6}$$

Similarly, the Nusselt numbers or friction factors can be obtained with equations (7) and (8) [10]:

$$Nu = 3.33\left(\frac{f_c}{2}\right)^{1.10}\left(\frac{D_i}{D}\right)^{0.061} Pr^{1/3} Re \tag{7}$$

$$\left[\left(\left(\frac{Nu}{Re\,Pr}\right)Pr^{2/3}\right)/3.33\left(\frac{D_i}{D}\right)^{0.061}\right]^{1/1.10} = \left(\frac{f_c}{2}\right) \tag{8}$$

Equations (5) to (8) are valid for 20000 < *Re* < 150000, $0.0123 \leq \frac{D_i}{D} \leq 0.2035$.

Kadivar et al. (2021) [34] used empirical correlations derived by Naphon (2016) [35] for heat transfer and pressure drop in spiral coils under turbulent flow conditions in their entropy analysis. The Nusselt number for turbulent single-phase nanofluid is given by equation (9) and the Darcy friction factor is given by equation (10).

$$Nu = 2.117 \cdot Re^{0.308} \cdot Pr^{-0.077} \cdot Cr^{-0.115} \cdot \phi^{0.068} \tag{9}$$

In equation (9) the curvature ratio $Cr = d_t/(R_{min} + R_{max})$ and $\boldsymbol{\phi}$ is the nanoparticle volume fraction.

$$f = 0.268 \cdot Re^{-0.736} \cdot Cr^{-1.042} \cdot \phi^{0.009} \tag{10}$$

The Nusselt number is valid for 4000 < *Re* < 9000; 4 < *Pr* < 7; 0.03 < *Cr* < 0.06; 0.01 % < $\boldsymbol{\phi}$ < 0.05 %.

5.2 Two-phase flow correlations

Decades of research from diverse experimental data have yielded correlations for horizontal and inclined straight smooth tubes, yet accuracy remains debated due to the complex two-phase condensation phenomena [36]. The combination of various two-phase flow patterns with the secondary flow phenomenon, driven by coil-induced centrifugal forces, makes it exceptionally challenging to conduct a flow field analysis of two-phase flow in coiled tubes [37]. Zhang et al. (2015) [38] and Blose et al. (2023) [39] identified the two-phase flow correlation by Cavallini et al. (2006) [40] as the best for predicting condensation heat transfer coefficients inside straight horizontal smooth tubes [38][39].

Cavallini et al. [40] recognised that a simpler method was required for subdividing the two-phase flow regimes. They proposed that the flow regimes should be subdivided based on the influence that certain parameters (including the fluid type, mass velocity, saturation temperature, vapour quality, and duct geometry) exert on the condensation heat transfer coefficient. The transition dimensionless vapour velocity, J_V^T is given by Equation (11).

$$J_V^T = \left\{ \left[\frac{7.5}{(4.3X_{tt}^{1.111} + 1)} \right]^{-3} + C_T^{-3} \right\}^{-1/3} \tag{11}$$

Where, $C_T = 1.6$ for hydrocarbons and, $C_T = 2.6$ for other refrigerants. The Martinelli parameter, X_{tt} is defined in Equation (12).

$$X_{tt} = \left(\frac{\mu_L}{\mu_G}\right)^{0.1} \left(\frac{\rho_G}{\rho_L}\right)^{0.5} \left[\frac{(1-x)}{x}\right]^{0.9} \tag{12}$$

In equation (12), μ is the dynamic viscosity with subscripts *L* and *G*, denoting liquid and gas. Similarly, ρ is the density and *x* is the thermodynamic vapor quality. The dimensionless vapour velocity, J_V (also known as the modified Froude number), is defined by Equation (13).

$$J_V = \frac{xG}{\sqrt{g d_i \rho_V (\rho_L - \rho_V)}} \tag{13}$$

In equation (13), *G* is the mass velocity, *g* is the standard gravitational acceleration, and d_i is the internal tube diameter. For $J_V > J_V^T$, where ΔT represents the independent flow regime, the correlation for annular flow is given by Equation (14).

$$h_A = h_{LO} \left[1 + 1.128\, x^{0.817} \left(\frac{\rho_L}{\rho_V}\right)^{0.3685} \left(\frac{\mu_L}{\mu_V} right\right)^{0.2363} \left(1 - \frac{\mu_V}{\mu_L}\right)^{2.144} Pr_L^{-0.1} \right] \tag{14}$$

In equation (14), h_A is the heat transfer coefficient of the temperature independent flow regime. h_{LO} is the heat transfer coefficient of the liquid phase with total flow. h_{LO} is the heat transfer coefficient of the liquid-only phase and is calculated using the Dittus-Boelter equation (15):

$$h_{LO} = 0.023 Re_{LO}^{0.8} Pr_L^{0.4} \tag{15}$$

For $J_V \leq J_V^T$, where ΔT is the dependent flow regime, the correlation for stratified flow is provided by equation (16)::

$$h = \left[h_A \left(\frac{J_V^T}{J_V}\right)^{0.8} - h_{STRAT} \right] \left(\frac{J_V}{J_V^T}\right) + h_{STRAT} \tag{16}$$

In equation (16), h_{STRAT} is the heat transfer coefficient stratified number, which is determined by Equation (17).

$$h_{STRAT} = 0.725 \left\{ 1 + 0.741 \left[\frac{1-x}{x}\right]^{0.3321} \right\}^{-1} \left(\frac{k_L^3 \rho_L \mu_L d_i \Delta T}{(\rho_L - \rho_G) g h_{LG}} \right)^{0.25} + h_{LO}(1 - x^{0.087}) \tag{17}$$

In equation (17), k is the thermal conductivity, ΔT is the temperature difference between T_S, the saturation temperature and T_W, tube internal wall temperature, h_{LG} is the latent heat. No heat transfer correlations are available in the literature for condensing in dimpled, fluted or other non-conventionally shaped spiral condensers. This leaves the designer with a dilemma. A 1D design methodology, depending on correlations such as those discussed above, assists the designer in producing a basic design for a specific heat transfer duty, that then can be

refined and optimised through experimentation or by employing computational fluid dynamics (CFD). In the absence of heat transfer correlations, the designer can use the most applicable correlations to produce an initial design, knowing that there will be a significant error margin. The design can then be experimentally characterised, and the heat transfer correlations can be adjusted so that they produce acceptable heat transfer coefficient results. This approach will be lengthy but should, if well executed, produce acceptable correlations. Contemporary CFD software is capable of simulation multi-phase flow and can be used to develop condensing flow heat transfer correlations for non-standard flow channels [41][42]. The CFD models will still have to be experimentally validated.

6 Conclusion

Metal AM is an attractive manufacturing technology for the production of compact heat exchangers. AM enables rapid production of complex components from CAD data that were once nearly impossible to manufacture with traditional methods. Compact stacked finned spiral-coil configurations is an attractive geometry for producing compact condensers for application in organic Rankine cycles.

It is important to recognise that in many scenarios, the intricacies of heat exchangers are influenced not only by performance requirements but also by the constraints and capabilities of the manufacturing process. While various AM processes offer significant advantages, the successful implementation of these technologies requires careful consideration of the process parameters, material selection, and post-production treatment. Challenges such as ensuring adequate surface finish, avoiding porosity, managing support structures and proper removal of unsintered powder from flow channels remain critical to realise the full potential of producing compact heat exchangers with AM.

A reliable thermo-hydraulic and mechanical design methodology is required to design and produce compact heat exchangers by means of AM. The thermo-hydraulic design methodology relies on accurate heat transfer correlations which in many cases are inadequate. This is the case for compact stacked finned spiral-coil condensers with non-standard flow channels. Reliable heat transfer and pressure drop correlations should be developed for compact finned spiral coil heat condensers. Reliable correlations will enable confident 1D thermo-hydraulic design of these condensers. In the absence of reliable correlations 1D designs should be based on currently available correlations discussed in this paper and should be adapted once experimental or CFD simulation results are available. 1D design methodology remains essential to develop a baseline design before it is refined and/or optimised through experimentation or with the aid of CFD analysis.

References

1. B. K. Hodge and R. Taylor, Analysis and Design of Energy Systems, 3rd ed., Pearson, 1998.
2. W. M. Kays and A. L. London, Compact Heat Exchangers, 3rd ed., 2018.
3. B. Zohuri, 'Heat Exchanger Types and Classifications,' in Compact Heat Exchangers, Springer Int. Publ., pp. 19–56, 2018, doi: https://doi.org/10.1007/978-3-319-29835-1_2.
4. W. S. Kim, 'Design optimization of cross-counter flow compact heat exchanger for energy recovery ventilator,' Int. J. Air-Cond. Refrig., 30(1), 2022, doi: https://doi.org/10.1007/s44189-022-00016-2.

5. J. S. Kwon, S. Son, J. Y. Heo, and J. I. Lee, 'Compact heat exchangers for supercritical CO_2 power cycle application,' Energy Convers. Manag., 209, 2020, doi: https://doi.org/10.1016/j.enconman.2020.112666.
6. K. Thulukkanam, Heat Exchanger Design Handbook, 2013.
7. Ameen, S. Mollik, G. Quadir, and K. N. Seetharamu, 'Investigation into the Phase Change of Refrigerant in a Wire–and–Tube Condenser of Refrigerator,' J. Teknol., 43, 2005, doi: https://doi.org/10.11113/jt.v43.756.
8. Zarei, S. Seddighi, S. Elahi, and R. Örlü, 'Experimental investigation of the heat transfer from the helical coil heat exchanger using bubble injection for cold thermal energy storage system,' Appl. Therm. Eng., 200, 2022, doi: https://doi.org/10.1016/j.applthermaleng.2021.117559.
9. Cihan, K. Kahveci, A. Tezcan, and O. Hacıhafızoğlu, 'Flow and Heat Transfer Around an Air-Cooled Coil Condenser,' in Proc. World Congr. Mech., Chem. Mater. Eng. (MCM), Paper No. 316, 2015.
10. R. H. Patil, 'Fluid flow and heat transfer analogy for laminar and turbulent flow inside spiral tubes,' Int. J. Therm. Sci., 139, pp. 362–375, 2019, doi: https://doi.org/10.1016/j.ijthermalsci.2019.01.036.
11. M. Fuchs, D. Heinrich, X. Luo, and S. Kabelac, 'Thermal performance measurement of additive manufactured high-temperature compact heat exchangers,' J. Phys.: Conf. Ser., 2021, doi: https://doi.org/10.1088/1742-6596/2116/1/012095.
12. K. Kanishka and B. Acherjee, 'Revolutionizing manufacturing: A comprehensive overview of additive manufacturing processes, materials, developments, and challenges,' J. Manuf. Process., 107, pp. 574–619, 2023, doi: https://doi.org/10.1016/j.jmapro.2023.10.024.
13. Kaur and P. Singh, 'State of the art in heat exchanger additive manufacturing,' Int. J. Heat Mass Transf., 178, 2021, doi: https://doi.org/10.1016/j.ijheatmasstransfer.2021.121600.
14. W. Beard, R. Lancaster, N. Barnard, T. Jones, and J. Adams, 'The influence of surface finish and build orientation on the low cycle fatigue behaviour of laser powder bed fused stainless steel 316L,' Mater. Sci. Eng. A, 864, 2023, doi: https://doi.org/10.1016/j.msea.2023.144593.
15. F. Careri, R. H. U. Khan, C. Todd, and M. M. Attallah, 'Additive manufacturing of heat exchangers in aerospace applications: a review,' Appl. Therm. Eng., 2023, doi: https://doi.org/10.1016/j.applthermaleng.2023.121387.
16. Durafintube, 'Finned Tube Heat Exchangers', 2025. Available: https://durafintube.com/product/bent-finned-tubes/
17. Dimpleflo, 'Dimpled tube profiles', 2025. Accessed: May 07, 2025. Available: https://www.dimpleflo.com/
18. N. Read, W. Wang, K. Essa, and M. M. Attallah, 'Selective laser melting of AlSi10Mg alloy: Process optimisation and mechanical properties development,' Mater. Des., 65, pp. 417–424, 2015, doi: https://doi.org/10.1016/j.matdes.2014.09.044.
19. M. Shange, I. Yadroitsava, S. Pityana, I. Yadroitsev, and A. Du Plessis, 'Determining the effect of surface roughness and porosity at different inclinations of LPBF parts,' in RAPDASA Conf. Proc., pp. 40–51, 2019.
20. S. C. Venter, G. G. Jacobs, and J. Du Preez, 'Design considerations for developing an additive manufactured Ti-6Al-4V compact counter-flow heat exchanger for application in organic Rankine cycles,' in RAPDASA Conf. Proc., pp. 192–200, 2018.

21. D. C. Bester and M. Shange, "Design for Additive Manufacturing: An Introduction to Design Rules and Constraints for High Speed SLM," in *RAPDASA Conf. Proc.*, pp. 413–420, 2019.
22. Protolabs, "How to Design and Manufacture Metal 3D-Printed Parts," Jun. 2021. [Online]. Available: https://www.protolabs.com/resources/design-tips/how-to-designand-manufacture-metal-3d-printed-parts/
23. EngineeringPage, "Tube Size and Wall Thickness for Heat Exchanger Tubes," 2025. [Online]. Available: https://www.engineeringpage.com/technology/thermal/tubesize.html
24. M. Kabir, T. Gemeda, E. Preller, and J. Xu, "Design and Development of a PCM-Based Two-Phase Heat Exchanger Manufactured Additively for Spacecraft Thermal Management Systems," *Int. J. Heat Mass Transf.*, vol. 180, Dec. 2021, doi: https://doi.org/10.1016/j.ijheatmasstransfer.2021.121782.
25. M. Cogho and D. Preez, "Design Lessons for Additive Manufactured Small Radial Flow Ti-6Al-4V Turbines for Application in Organic Rankine Cycles," in *RAPDASA Conf. Proc.*, pp. 207–218, 2018.
26. R. K. Shah and D. P. Sekulic, *Fundamentals of Heat Exchanger Design*, 2003.
27. Dabestani and M. Kahani, "CFD analysis of rotation effect on flow patterns and heat transfer enhancement in a horizontal spiral tube heat exchanger," *Case Stud. Therm. Eng.*, vol. 64, Dec. 2024, doi: https://doi.org/10.1016/j.csite.2024.105494.
28. L. N. Thanh and M. H. Nguyen, "Heat transfer and flow characteristics in horizontal spiral coils with flat tubes and rectangular ribs: CFD and optimization," *Int. J. Thermofluids*, vol. 26, Mar. 2025, doi: https://doi.org/10.1016/j.ijft.2025.101072.
29. F. Li, Z. Tian, Y. Jiang, W. Zheng, J. Chen, and S. Li, "Analysis of Flow and Pressure Drop on Tube Side of Spiral Tube Heat Exchanger under Sloshing Conditions," *Energies*, vol. 16, no. 14, Jul. 2023, doi: https://doi.org/10.3390/en16145263.
30. M. L. Dordevic, V. P. Stefanovic, and M. V. Mancic, "Pressure drop and stability of flow in Archimedean spiral tube with transverse corrugations," *Therm. Sci.*, vol. 20, no. 2, pp. 579–591, 2016, doi: https://doi.org/10.2298/TSCI150118212D.
31. S. Kakac, H. Liu, and A. Pramuanjaroenkij, *Heat Exchangers: Selection, Rating, and Thermal Design*, 3rd ed., Taylor & Francis Group, 2012.
32. P. Colburn, "A Method of Correlating Forced Convection Heat Transfer Data and a Comparison with Fluid Friction," *Trans. Am. Inst. Chem. Eng.*, vol. 29, pp. 174–210, 1933.
33. E. F. Schmidt, "Wärmeübertragung und Druckverlust in Rohrschlangen," *Chem. Ing. Tech.*, vol. 13, pp. 781–789, 1967.
34. M. Kadivar, M. Sharifpur, and J. P. Meyer, "Convection Heat Transfer, Entropy Generation Analysis and Thermodynamic Optimization of Nanofluid Flow in Spiral Coil Tube," 2021.
35. P. Naphon, "Experimental investigation the nanofluids heat transfer characteristics in horizontal spirally coiled tubes," *Int. J. Heat Mass Transf.*, vol. 93, pp. 293–300, 2016, doi: https://doi.org/10.1016/j.ijheatmasstransfer.2015.09.089.
36. R. D. E. Ewim, M. Mehrabi, and J. P. Meyer, "Modeling of Heat Transfer Coefficients during Condensation at Low Mass Fluxes Inside Horizontal and Inclined Smooth Tubes," 2021.
37. Yan, "Study of two-phase flow patterns and frictional pressure drop in helical and spiral coils," 1992. [Online]. Available: https://trace.tennessee.edu/utk_gradthes/12321
38. H. Zhang, X. Fang, H. Shang, and W. Chen, "Flow condensation heat transfer correlations in horizontal channels," *Int. J. Refrig.*, vol. 59, pp. 102–114, 2015, doi: https://doi.org/10.1016/j.ijrefrig.2015.07.013.

39. S. C. Blose, D. R. E. Ewim, A. C. Eloka-Eboka, and A. O. Adelaja, "Improved correlation for predicting heat transfer coefficients during condensation inside smooth horizontal tubes," *Int. J. Low-Carbon Technol.*, vol. 18, pp. 750–763, 2023, doi: https://doi.org/10.1093/ijlct/ctad052.
40. Cavallini et al., "Condensation in horizontal smooth tubes: A new heat transfer model for heat exchanger design," *Heat Transf. Eng.*, pp. 31–38, Sep. 2006, doi: https://doi.org/10.1080/01457630600793970.
41. Y. Lei, I. Mudawar, and Z. Chen, "Computational and experimental investigation of condensation flow patterns and heat transfer in parallel rectangular micro-channels," *Int. J. Heat Mass Transf.*, vol. 149, p. 119158, 2020, doi: https://doi.org/10.1016/j.ijheatmasstransfer.2019.119158.
42. N. Padoin and C. Soares, "CFD Modeling of Steam Condensation in Industrial Pipes," May 2014, doi: 10.13140/RG.2.1.1900.9044.